Tellus (2003), 55B, 547–554
Printed in UK. All rights reserved

TELLUS
ISSN 0280–6509

Sensitivity of inter-annual variation of CO_2 seasonal cycle at Mauna Loa to atmospheric transport

By SHOICHI TAGUCHI[1]*, SHOHEI MURAYAMA[1] and KAZ HIGUCHI[2], [1]*National Institute of Advanced Industrial Science and Technology, AIST-West, 16–1, Onogawa, Tsukuba, Ibaraki 305–8569, Japan;* [2]*Meteorological Service of Canada, 4905 Dufferin Street, Toronto, Ontario M3H 5T4, Canada*

(Manuscript received 25 January 2002; in final form 12 September 2002)

ABSTRACT

Origins of the inter-annual variations of the Mauna Loa atmospheric CO_2 seasonal cycle related to atmospheric transport were examined using a global atmospheric transport model with prescribed land biota CO_2 source functions at 11 land sections. On average, the seasonal variation of atmospheric CO_2 at Mauna Loa is influenced mostly by the Siberian CO_2 flux, followed by temperate Asia and North America. The inter-annual variability of the seasonal cycle is caused mainly by the inter-annual variation in the transport of the Siberian signal to Mauna Loa. The characteristics of the simulated seasonal cycle and its inter-annual variability at Mauna Loa are found to be sensitive to the quality of the wind data used to drive the transport model. Implication of this result is that for studying a long-term variations of atmospheric transport a meteorological data set for driving an atmospheric transport model should be obtained from the same production procedure.

1. Introduction

The atmospheric CO_2 seasonal cycle is driven primarily by the photosynthesis–respiration annual cycle of the land ecosystems. Inter-annual variations in the seasonal cycle have been attributed mostly to the year-to-year changes in the activities of the land biosphere (e.g. Keeling et al., 1996; Myneni et al., 1997). However, recent modeling studies (e.g., Dargaville et al., 2000; Higuchi et al., 2002) have indicated that the inter-annual variations in the atmospheric transport make a significant contribution to the inter-annual variations of atmospheric CO_2 seasonal cycle, particularly in relation to its amplitude. Higuchi et al. (2002) also showed that changes in the atmospheric circulation regime could account for a significant portion of quasi-decadal changes in the Northern Hemisphere atmospheric CO_2 seasonal cycle amplitude observed over the last 20 years.

*Corresponding author.
e-mail: s.taguchi@aist.go.jp

The wind data used by Higuchi et al. (2002) to drive a three-dimensional (3-d) transport model were obtained from the European Centre for Medium-Range Weather Forecasts (ECMWF); they used reanalysis data from 1979 to 1991, and operational data from 1992 to 1998. In the present study we used the same transport model but drove it with reanalysis data for the period 1979–1993, and with operational data for the period 1994–1999. The issue of the difference in the source of the wind data for 1992 and 1993 between this study and that of Higuchi et al. (2002) was examined within the context of its impact on the simulated Mauna Loa seasonal cycle amplitude and on the differentiation of the land CO_2 source function signature transported to Mauna Loa. We will show that the actual year-to-year change in the simulated seasonal cycle amplitude depends greatly on the “quality” of the wind data, i.e. the way they are generated and archived. The robustness of the results of Higuchi et al. (2002) can only be shown if the transport model driven by other “observed” wind data produces similar results. This issue is important because metabolic response of the land biosphere to climate change does have a significant effect on the global carbon cycle, and it is critical that we quantify this since the effect will influence regulatory strategies of CO_2 emissions in the future.

2. Model and observations

Observed concentrations used in this study were daily averages compiled by the National Oceanic and Atmospheric Administration, Climate Monitoring and Diagnostics Laboratory (Conway et al., 1994), and were acquired from the Web site (ftp://ftp.cmdl.noaa.gov/ccg).

The atmospheric transport model used in this study was NIRE-CTM-96 (Taguchi et al., 2002a,b). It has 2.5° horizontal resolution and 15 vertical levels up to about 30 km. Transport is calculated by using semi-Lagrangian method. The number of levels in the planetary boundary layer depends on the depth of mixed layer estimated from the bulk-Richardson number (Taguchi, 1996).

The wind data to drive this transport model were obtained from the European Centre for Medium Range Weather Forecasts (ECMWF), and were made up of data derived from both reanalysis and operational analysis. The data in our possession are summarized in Table 1. The T47 data set contains the European Centre Reanalysis basic upper air data from 1979 to 1993. These wind data were generated by a two-step procedure. The original data archived in 106-wave number triangular truncation were degraded in resolution to 47-wavenumber triangular truncation, and then sampled at a $2.5 \times 2.5°$ grid resolution (Keith Fielding, personal communication). The T213 and T63 data sets were obtained from the operational analysis, each set derived with different analysis procedure. The T213 upper-air data set (1992–1994) was obtained from the ECMWF/TOGA advanced operational analysis in which the data were sampled at a $2.5 \times 2.5°$ grid resolution directly from the 213 triangular truncation spectral archive. The T63 data set (1995–1999), on the other hand, was obtained from the ECMWF operational atmospheric model archive (http://www.ecmwf.services/data/archives) derived by sampling an intermediate spectral truncation of triangular 63 resolution, degraded from a triangular 213 or 319 spectral archive.

Table 1. *ECMWF wind data available to the study*

Data set	Years available
T47	1979–1993
T213	1992–1994
T63	1995–1999
Data used in Higuchi et al. (2002) study	
T47	1979–1991
T213	1992–1994
T63	1995–1998
Data used in this study	
T47	1979–1993
T213	1994
T63	1995–1999

In this study, we used T47 (1979–1993), T213 (1994) and T63 (1995–1999). As shown in Table 1, the only difference in the wind data used to drive the model between this study and that of Higuchi et al. (2002) is the 2-yr period (1992 and 1993) during which we used T47 of the reanalysis data, instead of the T213 operational analysis data.

Southern oscillation index (SOI) was used to detect the period of El Niño. The data were obtained from the Bureau of Meteorology, Australia (http://www.bom.gov.au).

3. Experiment

Monthly mean CO_2 fluxes from the land biota had no inter-annual variations and were derived from the Carnegie Ames Stanford Approach (CASA) biosphere model (Potter et al., 1993, Randerson et al., 1997). In accordance with the TransCom Phase 3 protocol (Gurnery et al., 2002), the global land biosphere was divided into 11 sections (Fig. 1), each with its own characteristic seasonal CO_2 flux cycle (Fig. 2). Boreal Asia has the largest emissions. Temperate North America, temperate Asia and Europe have absorption in May–August and small emissions in other months. South America and South Africa have similar seasonal cycles. The phase of the seasonal fluxes in the Southern Hemisphere is opposite to that of the seasonal fluxes in the Northern Hemisphere. Since the fossil fuel CO_2 emission and the net air–sea flux of CO_2 show only a minor seasonal variation, making relatively small contributions to the observed atmospheric CO_2 seasonal cycle, they were not included as part of the CO_2 forcing function

The model integration was initiated with a uniform CO_2 distribution of 350 ppm (parts per million) in the atmosphere. The initialization of the model included

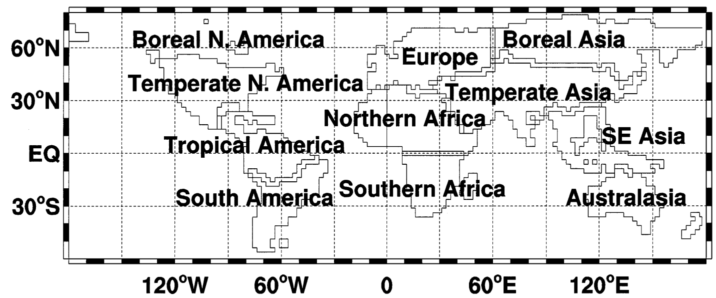

Fig. 1. Land sections specified for emissions. Boreal North America (1), temperate North America (2), tropical America (3), South America (4), Northern Africa (5), Southern Africa (6), Boreal Asia (7), temperate Asia (8), tropical Asia (9), Australia (10) and Europe (11).

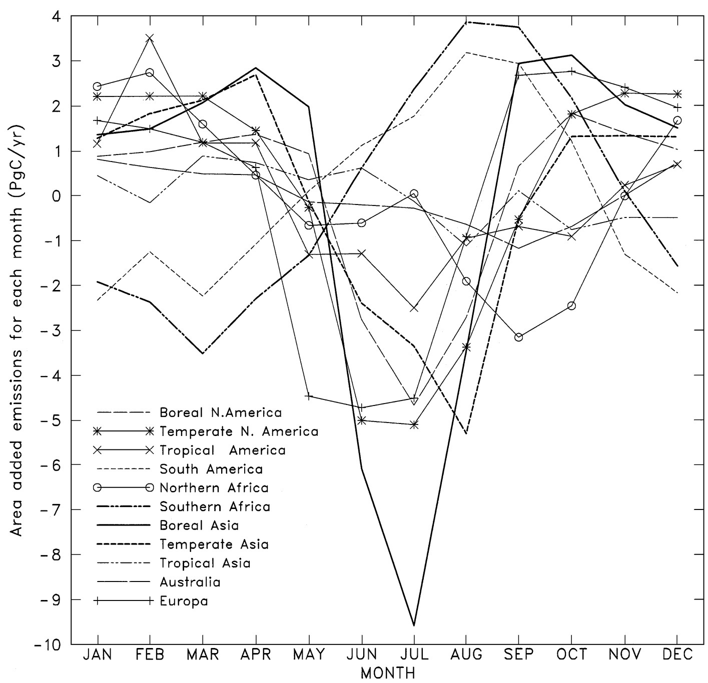

Fig. 2. Monthly emissions and absorptions added over each land section. Units are in Pg C yr^{-1}. The size of emission and absorption depend on the rate of emission and absorption and also the size of section. The emission and absorption strength at each grid were adjusted to balance within 0.01% of the total emissions or absorptions (equivalent to the growing season net flux).

running the first year of the model twice with the 1979 meteorological fields.

4. Results and discussion

Amplitude of a seasonal cycle in any calendar year was defined as the peak-to-trough difference in the smooth curve (composed of three trigonometric harmonic components with periods of 12, 6 and 4 months) fitted to the CO_2 concentration values. This definition was applied to both the observed and model data.

An amplitude time series calculated using the observed data from Mauna Loa is shown in Fig. 3. Also shown are the amplitudes calculated from model simulations using (1) T47 (1979–1993) and T63

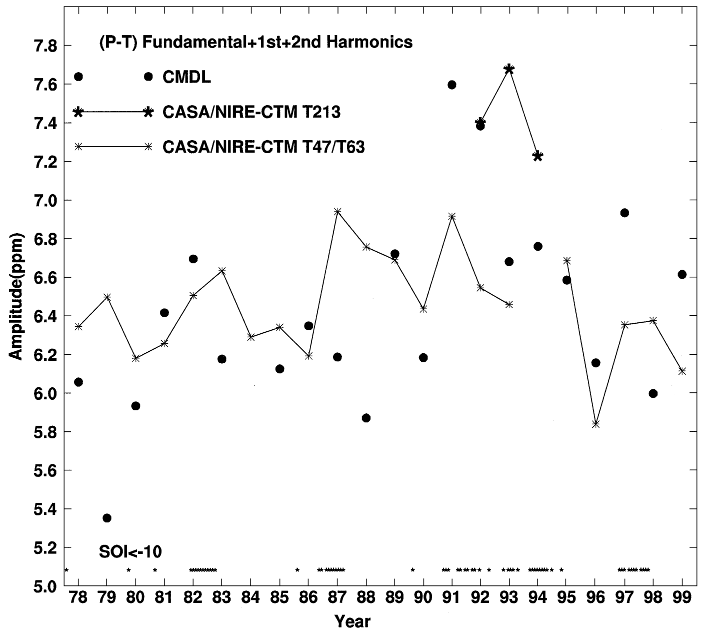

Fig. 3. Amplitudes of CO_2 at Mauna Loa simulated by a global atmospheric transport model (NIRE-CTM-96/ECMWF) combined with sources and sinks of CO_2 derived from the CASA land ecosystem model. Also shown is the amplitude estimated from the observations (CMDL). Results of the simulations using European Centre Reanalysis (ERA) and European Center Operational Archive (TOGA) are shown separately. Note that the periods 1992–1994 and 1995–1999 are not connected because the model used different wind data. See text and Table 2 for details.

(1995–1999) wind values, and (2) T213 (1992–1994) wind values. The T213 integration was initiated at the end of 1991 and terminated at the end of 1994. The amplitude value for 1984 is not plotted because there were periods with longer than a month of missing CO_2 data. Also shown at the bottom of the figure are the monthly values of the Southern Oscillation Index (SOI) with magnitude less than –10.

Overall, the magnitude of the inter-annual variability (i.e. standard deviation) in the seasonal cycle amplitude produced by changes in the atmospheric circulation in the model is comparable to that which is observed at Mauna Loa. However, there is less agreement in the actual year-to-year variation of the magnitude and phase of the amplitude, with a correlation of 0.25 (not statistically significant) between the observed and simulated time series.

Trends in the amplitude are summarized in Table 2. Agreement between the observed and the simulated tendencies in amplitude change is found only during certain periods, such as 1980–1982, 1989–1993 and 1995–1997. In other periods, such as 1982–1983 and 1986–1987, the observed trend is in the

Table 2. *Tendency of amplitude for observations and model simulations*

Year	Observation	Model
79–80	+	−
80–81	+	+
81–82	+	+
82–83	−	+
83–84	N/A	−
84–85	N/A	+
85–86	+	−
86–87	−	+
87–88	−	−
88–89	+	−
89–90	−	−
90–91	+	+
91–92	−	−
92–93	−	−
93–94	+	N/A
94–95	−	N/A
95–96	−	−
96–97	+	+
97–98	−	+
98–99	+	−

opposite direction to that of the simulated trend. The coincidence of these latter two periods (1982–1983 and 1986–1987) with the SOI indicates that an occurrence of an El Niño event in the tropical Pacific could contribute significantly to the observation of anomalous seasonal cycle amplitude at Mauna Loa, leading to the disagreement in the tendency in the amplitude trend during these periods between the observed and the simulated. It has been found that an ENSO event causes global anomaly in the distribution of land biospheric and oceanic sources and sinks of CO_2 (Rayner et al., 1999). It is interesting to note, however, that in periods around 1991, 1993 and 1997 when the SOI < -10, there is agreement between the observed and simulated tendency in the seasonal cycle amplitude change. A reason for this is that the evolution of a characteristic El-Niño anomaly may be different from case to case. For example, different responses in the land biosphere might be expected due to differences in the timing of the El-Niño initiation from event to event. Also, eruption of Mt. Pinatubo possibly modulated the seasonal flux of land biosphere.

It is also evident in Fig. 3 that the seasonal cycle amplitudes of 1992 and 1993 produced by the model during the T47 wind data are significantly different from those produced using the T213 wind data. The difference in the meteorological fields between these two data sets, which can generate such marked differences in the seasonal cycle amplitude, will be discussed later in the section.

Amplitudes of seasonal cycles simulated for Mauna Loa from CO_2 flux sources at 11 land sections are shown in Fig. 4. Boreal Asia produced the largest amplitudes throughout the period of integration, followed by Temperate Asia, Temperate North America and Europe. If we divide the period 1979–1993 during which only the T47 winds were used to drive the model, into two sub-periods 1979–1986 and 1987–1993, the amplitude produced by the Boreal Asian biosphere was greater during the latter sub-period than the former. Table 3 lists mean and standard deviations of the amplitudes estimated for these two sub-periods. The difference in the observed mean amplitude between the two sub-periods is not statistically significant. However, the model simulation indicates that, had the Mauna Loa CO_2 seasonal cycle amplitude been influenced by changes in atmospheric transport alone from 1979 to 1993, there is a statistically significant difference in the amplitude change between the two sub-periods. Figure 4 and Table 3 show that

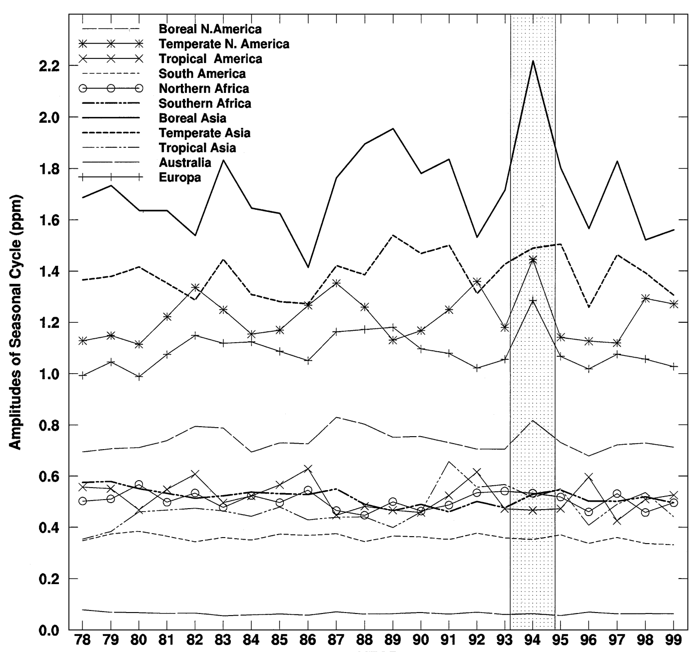

Fig. 4. Amplitude of seasonal cycle simulated at Mauna Loa using emissions and absorptions at 11 land sections. Results for 1994 is shaded to highlight the fact that it was the only year in which the model was driven by the T213 wind data.

Table 3. *Mean and standard deviation of amplitudes for the two periods, 1979–1986 and 1987–1993 (in ppm.)*

	1979–1986		1987–1993	
	Mean	STD	Mean	STD
Peak to trough				
Observation	6.14	0.40	6.66	0.6
Simulation	6.36	0.16	6.68	0.2
Sections				
Boreal N. America	0.736	0.034	0.754	0.044
Temperate N. America	1.208	0.068	1.242	0.082
Tropical America	0.548	0.050	0.494	0.054
South America	0.366	0.012	0.362	0.010
North Africa	0.520	0.028	0.490	0.034
Southern Africa	0.538	0.018	0.490	0.028
Boreal Asia	1.632	0.116	1.782	0.128
Temperate Asia	1.342	0.062	1.436	0.070
SE Asia	0.450	0.030	0.502	0.086
Australasia	0.062	0.004	0.066	0.004
Europe	1.080	0.048	1.110	0.058

this transport-only contribution is caused mainly by the change in the Boreal Asia amplitude. This leads us to conclude that the growth in CO_2 seasonal cycle amplitude at Mauna Loa in the simulation from 1979–1986 to 1987–1993 was caused likely by a change in atmospheric circulation which allowed Mauna Loa to come increasingly under the influence of biospheric CO_2 signal from Boreal Asia. Variations in the observed amplitudes in 1986–93 indicate that sources and sinks of either land or ocean might be changed significantly in this period.

Overall, amplitudes from the tropical regions were relatively minimal, since the seasonal CO_2 flux cycle is minimal there. The year 1994 is shaded, to point out the fact that it is the only year in which we used the T213 meteorological data, which are inconsistent with T47 and T63 data. Therefore, the peak in amplitude shown for 1994 in Fig. 4 could be artificial.

As an example of how the seasonal cycle amplitude at Mauna Loa can be influenced by changes in

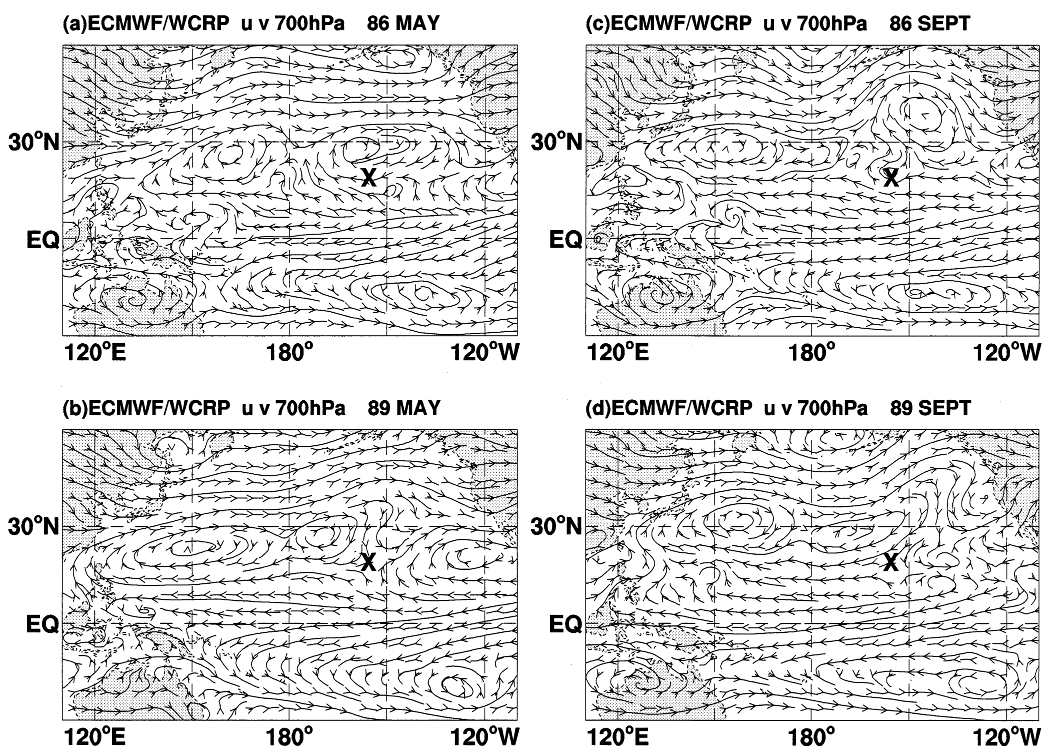

Fig. 5. Stream lines for monthly mean winds at 700 hPa. (a) May 1986, (b) May 1989, (c) September 1986 and (d) September 1989. Cross indicates the location of Mauna Loa.

atmospheric transport, we chose 1986 and 1989 in Fig. 4. We can demonstrate this meteorologically. Figure 5 shows the stream lines of monthly mean winds in May and September at 700 hPa for 1986 and 1989. (Since the seasonal cycle amplitude is calculated as the difference between the maximum and minimum concentration values in any particular year, its magnitude is sensitive to the values in May and September when maximum and minimum concentrations, respectively, usually occur at Mauna Loa.) In 1986, predominant winds at Mauna Loa were easterly both in May and September. On the other hand, in 1989 they were westerly or northerly in May and September, indicating a faster transport of air mass from high latitudes sources and sinks.

The differences in two data sets produced from different procedures are demonstrated in Fig. 6, although the relationship between these differences and amplitudes is not clear. Statistics of vertical velocity at 700 hPa for two meteorological data sets, T47 and

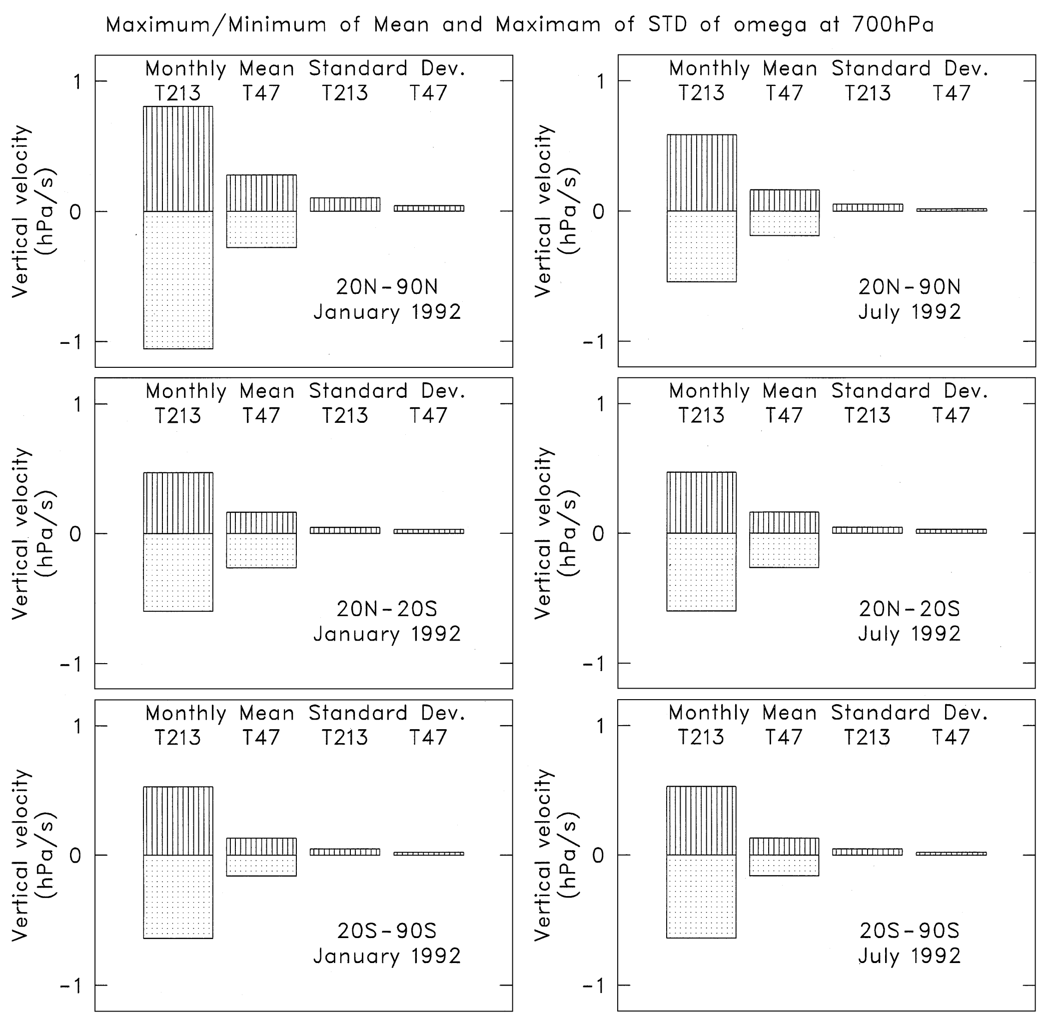

Fig. 6. Maximum and minimum of monthly mean vertical velocity of meteorological data used in the transport model. Maximum of standard deviations derived from 6 hourly dataset are also shown for two months. Two datasets of 2.5° resolution sampled at T213 (Operational) and T47 (ERA) are compared for the same period (January and July 1992) at the 700 hPa level. Statistics are taken at three latitude bands of 20°N–90°N (upper), 20°S–20°N (middle) and 90°S–20°S (bottom).

T213, for 1992 are shown for three latitude bands, 20°N–90°N, 20°N–20°S, 20°S–90°S and for January and July. In each box, extreme values of monthly mean vertical velocity and maximum of standard deviations are shown for the two data sets.

Maximum and minimum of monthly mean vertical velocities were obtained at the slope of large-scale mountains. Large standard deviations were also obtained at the slope. The magnitudes of mean vertical velocity were reduced significantly in T47, while standard deviations were not changed. In the tropics, standard deviations in T47 were larger than those in T213 at most areas (not shown). Therefore vertical transport by cumulus convections in the Inter-Tropical Convergence Zone might be enhanced in T47. These contrasting features might be caused by the differences in the parameterizations of physical processes in the numerical prediction models.

Similar differences may be anticipated in T213 and T47/T63 at 1994. This is the reason why the result of 1994 was partially shaded in Figs. 3 and 4.

5. Conclusions

Inter-annual variations of amplitudes obtained in the simulations were as large as those observed, indicating direct interpretation of changes in the observed atmospheric CO_2 seasonal cycle as a function of changes in carbon sources and sinks, without taking into account changes in atmospheric circulation regimes, is not appropriate. Furthermore, a meteorological data set for driving an atmospheric transport model must be obtained from the same production procedures because model simulations of inter-annual variations of atmospheric CO_2 seasonal cycle are sensitive to the quality of the wind fields.

6. Acknowledgements

We are indebted to Keith Fielding for information on the production process of $2.5 \times 2.5^{\circ}$ meteorological data in the ECMWF.

REFERENCES

Conway, T. J., Tans, P. P., Waterman, L. S., Thoning, K. W., Kitzis, D. R., Masarie K. A. and Zhang, N. 1994. Evidence for interannual variability of the carbon cycle from the National Oceanic and Atmospheric Administration/Climate Monitoring and Diagnostics Laboratory Global Air Sampling Network, *J. Geophys. Res.* **99**, 22831–22855.

Dargaville, R. J., Law, R. M. and Pribac, F. 2000. Implications of interannual variability in atmospheric circulations on modeled CO_2 concentrations and source estimates. *Global Biogeochem. Cycles* **14**, 931–943.

Gurnery, K. R., Law, R. M., Denning, A. S., Rayner, P. J., Baker, D., Bousquet, P., Bruhwiler, L., Chen, Y. H., Ciais, P., Fan, S., Fung, I. Y., Gloor, M., Heimann, M., Higuchi, K., John, J., Maki, T., Maksyutov, S., Masarie, K., Peylin, P., Prather, M., Pak, B. C., Randerson, J., Sarmiliento, J., Taguchi, S., Takahashi, T. and Yuen, C. W. 2002. Robust regional estimates of annual mean CO_2 sources and sinks. *Nature* **415**, 626–629.

Higuchi, K., Murayama, S. and Taguchi, S. 2002. Quasi-decadal variation of the atmospheric CO_2 seasonal cycle due to atmospheric circulation changes: 1979–1998. *Geophys. Res. Lett*. **29**, 10.1029/2001GL013751.

Keeling, C. D., Chin, J. F. S. and Whorf, T. P. 1996. Increased activity of northern vegetation inferred from atmospheric CO_2 measurements. *Nature* **382**, 146–149.

Myneni, R. B., Keeling, C. D., Tucker, C. J., Asrar, G. and Nemani, R. R. 1997. Increased plant growth in the northern high latitudes from 1981 to 1991. *Nature* **386**, 698–702.

Potter, C. S., Randerson, J. T., Field, C. B., Matson, P. A., Vitousek, P. M., Mooney, H. A. and Klooster, S. A. 1993. Terrestrial ecosystem production: A process model based on global satellite and surface data. *Global Biogeochem. Cycles* **7**, 811–841.

Randerson, J. T., Thompson, M. V., Conway, T. J., Fung, I. Y. and Field, C. B. 1997. The contribution of terrestrial sources and sinks to trends in the seasonal cycle of atmospheric carbon dioxide. *Global Biogeochem. Cycles* **11**, 535–560.

Rayner, P. J., Law, R. M. and Dargaville ?? 1999. The relationship between tropical CO_2 fluxes and the El Niño-Southern Oscillation. *Geophys. Res. Lett*. **26**, 493–496.

Taguchi, S. 1996. A three-dimensional model of atmospheric CO_2 transport based on analyzed winds: Model description and simulation results for TRANSCOM. *J. Geophys. Res.* **109**, 15099–15109.

Taguchi, S., Matsueda, H., Inoue, H. Y. and Sawa, Y. 2002a. Long-range transport of carbon monoxide from tropical ground to upper troposphere: a case study for South East Asia in October 1997. *Tellus* **54B**, 22–40.

Taguchi, S., Iida, T. and Moriizumi, J. 2002b. Evaluation of the atmospheric transport model NIRE-CTM-96 by using measured radon-222 concentrations. *Tellus* **54B**, 250–268.